catalysts

MDPI

Article

Biofuel Synthesis from Sorbitol by Aqueous Phase Hydrodeoxygenation over Bifunctional Catalysts: In-depth Study of the Ru–Pt/SiO_2–Al_2O_3 Catalytic System

Davina Messou, Laurence Vivier, Christine Canaff and Catherine Especel *

CNRS UMR 7285 IC2MP, Institut de Chimie des Milieux et des Matériaux de Poitiers, Université de Poitiers, 4 rue Michel Brunet, TSA 51106, 86073 Poitiers CEDEX 9, France; davina.messou@gmail.com (D.M.); laurence.vivier@univ-poitiers.fr (L.V.); christine.canaff@univ-poitiers.fr (C.C.)

* Correspondence: catherine.especel@univ-poitiers.fr; Tel.: +33-549453994

Received: 6 December 2018; Accepted: 27 January 2019; Published: 2 February 2019

Abstract: The catalytic performances of Ru–Pt/SiO_2–Al_2O_3 catalysts synthetized by three methods (co-impregnation (CI), successive impregnations (SI) and redox deposition (CR)) were compared for their sorbitol transformation to hexane under hydrothermal conditions. The existence of Pt–Ru interaction was demonstrated by TEM-EDX only on SI and CR samples, with a PtRu alloy suspected by XRD and XPS. The chemical nature of the Ru species differed according to the synthesis method with the presence of Ru^{4+} species on SI–(Ru–Pt) and CR catalysts. The SI–(Ru–Pt)/SiO_2–Al_2O_3 system displayed the best metal–acid function balance leading to the highest selectivity to hexane. The study of the reactivity of isosorbide and 2,5-dimethylfuran intermediates highlighted that the first one was poorly reactive compared to the second one, and the latter was selectively convertible to hexane. The synergy effect on SI– (Ru–Pt)/SiO_2–Al_2O_3 catalyst was attributed to the presence of small-sized bimetallic particles favoring an electronic exchange from Ru to Pt, and increasing the formation of 2,5-dimethylfuran.

Keywords: Sorbitol; Bimetallic catalyst; Platinum; Ruthenium; Alkanes production

1. Introduction

Biomass and more specifically lignocellulose have become important feedstocks for the production of chemicals, materials and fuels, because of the increasing price and the shortage of petroleum and global warming [1–7]. Lignocellulosic biomass that contains cellulose, hemicellulose and lignin, is abundant in the form of agricultural and forest residues. Contrary to petroleum which is underfunctionalized, biomass is overfunctionalized, and the removal of functionalities, particularly the oxygenated functions, is required via hydrodeoxygenation steps [8]. However, hydrodeoxygenation performed by liquid-phase processing (with water as solvent generally) has rarely been used in industrial chemistry until now, implying the need to develop actively new effective catalytic systems.

In the field of biomass valorisation, the aqueous phase hydrodeoxygenation (APHDO) of sorbitol is considered as an attractive route since this biomass-derived sugar alcohol, of high availability, is known as one of the 12 important target chemicals in the biomass program of the US Department of Energy [9,10]. Nevertheless, sorbitol remains one of the biomass-derived polyols with the most complex structure that drives difficult the understanding of its chemical transformation mechanism [11,12]. Dumesic and coll first studied the transformation of sorbitol in aqueous phase using a Pt/alumina catalyst initially with the aim to produce hydrogen (reforming process) [13]; further, this process was oriented to the production of valuable alkanes (C6 and C5) using a bifunctional

catalyst combining a metal phase (platinum) on an acidic support (silica–alumina) [14]. In 2010, Li and Huber identified several intermediates during the APHDO of sorbitol over a $Pt/SiO_2–Al_2O_3$ catalyst [15]. Then in 2013, Moreno et al. continued the investigations and proposed a relatively detailed reaction scheme for the sorbitol transformation, involving more than 30 products formed by the combination of several types of reactions [16]. According to this scheme, the selective transformation of sorbitol into hexane can occur by two routes: (i) an initial dehydration of sorbitol to sorbitan (1,4-anhydrosorbitol), then to isosorbide, followed by four successive dehydration-hydrogenation reactions leading to hexane; (ii) an initial dehydration to 2,5-dimethylfuran (2,5-DMF), followed by hydrogenation to 2,5-dimethyltetrahydrofuran (2,5-DMTHF), hydrogenolysis to 2-hexanol and finally dehydration–hydrogenation to hexane.

The support of the bifunctional catalysts was described to be active by its acidic sites (mainly Brønsted sites) catalyzing dehydration reactions, whereas the metallic sites can be implied in various reactions to favor (hydrogenation) or to limit (C-C bond cleavage) [17,18]. The proximity of the acidic and metallic sites does not seem to be a deciding factor in the mechanism since Dumesic and coll demonstrated that a $Pt/SiO_2–Al_2O_3$ catalyst and a Pt/Al_2O_3 one mixed with $SiO_2–Al_2O_3$ had the same selectivity for the same ratio of Pt sites/acidic sites [13,14]. Generally, dehydration is described as the rate-limiting step during the dehydration/hydrogenation process [19].

During catalytic processes of transformation in the aqueous phase, the product selectivity can be tuned depending on the nature of the metal, of the support and also of the promoter involved in the catalyst formulation [4]. It is well known that combining additional metals to monometallic catalysts can modify the surface properties to improve catalytic activity and selectivity to the desired product, and can increase the catalyst stability. Even if some authors reported the modification of supported monometallic Pt catalysts by different additives such as Ru, Re, Os, Ir, Ni, Co or Fe [20–24], the potentiality of bimetallic Pt-based catalysts remains a major challenge to selectively convert sorbitol to biofuels via the APHDO process.

In a previous work [25], we highlighted the efficiency of $Ru–Pt/SiO_2–Al_2O_3$ bimetallic catalysts to transform the sorbitol selectively into hexane in the aqueous phase. The actual paper follows on from this previous study. New $Ru–Pt/SiO_2–Al_2O_3$ bimetallic samples were prepared by different methods; all the gathered catalysts were characterized in-depth and their catalytic performances were compared in order to identify the best formulation in terms of hexane yield. Finally, complementary tests were performed with reactional intermediates in order to better understand the reactivity of these catalytic systems.

2. Results and Discussion

2.1. Characteristics of the Metal Function

The silica–alumina "SIRAL 40" from Sasol (noted S40) containing 60 wt.% Al_2O_3 and 40 wt.% SiO_2 was used as the support. The main characteristics of all the studied bimetallic Ru–Pt catalysts after activation (as well as those of the monometallic 3 wt.% Pt/S40 and 3wt.% Ru/S40 samples) are gathered in Table 1, i.e., physicochemical properties determined by N_2 sorption (specific surface area, pore volume and pore diameter) and the average particle size measured by TEM. In a previous work [25], we initiated a study on the effect of the preparation method of bimetallic Ru–Pt/S40 catalysts on their performances for the aqueous phase transformation of sorbitol. For that purpose, we had prepared the three bimetallic samples CI-(Ru-Pt)/S40 (entry 3), SI-(Ru-Pt)/S40 (entry 4) and CR-(Ru-Pt)/S40 (entry 6) containing all the same metallic contents in order to keep this parameter constant, i.e., 3 wt.% Ru and 3 wt.% Pt, but prepared by three different ways (co-impregnation CI, successive impregnation SI and catalytic reduction deposition CR). In the actual study, we completed the series with four new samples: (i) a new SI catalyst labelled SI–(Pt–Ru)/S40 (entry 5), loading with 3 wt.% Pt and 3 wt.% Ru and prepared by successive impregnation, but this time starting from a monometallic Ru/S40 sample before impregnating the Pt precursor salt, (ii) three new CR catalysts labelled CR-(x%Ru-Pt)/S40 (with

x = 2, 1 or 0.5 wt.% Ru; entries 7 to 9) synthesized by catalytic reduction deposition between the 3 wt.% Pt/S40 parent catalyst and the Ru precursor salt. In this latter case, the deposited Ru content has been deliberately diminished due to the fact the redox process is based on the following reaction: 3 Pt-H_{ads} + Ru^{3+} → $Ru^0(Pt)_3$ + 3 H^+ [26]. Three accessible Pt atoms chemisorbing hydrogen on the parent Pt/S40 catalyst are then needed to reduce one oxidized ruthenium atom introduced to the solution. Taking into account the metallic accessibility to hydrogen of the parent catalyst (85%, given in Reference [25]), the maximum Ru content needed to cover each surface platinum atom, i.e., to obtain a Ru monolayer, would be equal to 1.32 wt.%, so lesser than the 3 wt.% content deposited on the firstly-prepared CR catalyst.

Table 1. Properties of the Ru–Pt/S40 bimetallic catalysts prepared by co-impregnation (CI), successive impregnations (SI) or catalytic reduction deposition (CR), and of the corresponding monometallic samples. (The metallic loading of Pt and Ru is 3 wt.% unless otherwise indicated).

Entry	Catalysts/S40	Ru/Pt [1] (Atomic Ratio)	S_{BET} [2] ($m^2\ g^{-1}$)	V_P [2] ($cm^3\ g^{-1}$)	D_P [2] (nm)	đ [3] (nm)	Reference
1	Pt	-	392	0.84	8.2	1.1	Ref. [25]
2	Ru	-	362	0.83	8.7	28.0	Ref. [25]
3	CI–(Ru–Pt)	1.9	327	0.67	8.2	1.0 (Pt) 33.0 (Ru)	Ref. [25]
4	SI–(Ru–Pt)	1.9	300	0.72	8.6	2.3	Ref. [25]
5	SI–(Pt–Ru)	1.9	331	0.68	8.3	26.0	
6	CR–(Ru–Pt)	1.9	343	0.80	9.1	2.6	Ref. [25]
7	CR–(2%Ru–Pt)	1.3	366	0.77	8.4	n.d.	
8	CR–(1%Ru–Pt)	0.6	331	0.66	8.1	3.8	
9	CR–(0.5%Ru–Pt)	0.3	336	0.81	9.5	n.d.	

[1] Calculated from the metallic weight contents determined from elemental analysis. [2] Specific surface area S_{BET}, pore volume V_P and pore diameter D_P determined by N_2 sorption measurements. Values for the lone S40 support: S_{BET} = 510 $m^2\ g^{-1}$, V_P = 0.90 $cm^3\ g^{-1}$, D_P = 9.0 nm. [3] Average particles size determined by TEM analysis. n.d.: Not determined.

The prepared bimetallic catalysts display on the whole a lower specific surface area compared to the monometallic samples, which is in accordance with their higher global metal content. According to the preparation method (CI, SI or CR), their textural properties differ slightly, resulting from various undergone preparation and activation treatments and/or various locations and morphologies of the metallic particles on the support. Indeed, the three preparation methods lead to bimetallic Ru–Pt catalysts with different morphologies revealed by TEM-EDX analyses, which can be summarized as follows:

i. The CI bimetallic catalyst (entry 3) displays two populations of particles coexisting separately on the support (representative TEM pictures were given in Reference [25]): The first one with small sizes (around 1.0 nm) associated to a Pt phase and a second one constituted of Ru large particles (between 10.0 and 40.0 nm, leading to average size of 33.0 nm). This configuration is in line with the respective populations observed on both Pt/S40 and Ru/S40 monometallic samples that were also previously published [25].

ii. The SI–(Ru–Pt)/S40 catalyst (entry 4) exhibits bimetallic particles well dispersed on the support with relatively homogeneous sizes (average diameter of 2.3 nm, see TEM images in Reference [25]), as on the Pt/S40 monometallic sample. The newly-prepared SI system corresponding to an inverted order of impregnation (SI–(Pt–Ru)/S40, entry 5) leads to a rather large distribution of particles size as observed on the TEM image of Figure 1a (leading to an average diameter of 26.0 nm). This distribution is similar to that of the monometallic Ru/S40 sample. Moreover, EDX analysis reveals the presence of bimetallic particles constituted of variable composition functions of their size (starting from 50%$_{atom}$ to 95%$_{atom}$ Ru for the largest particles).

iii. For the CR–(Ru–Pt)/S40 catalyst (entry 6), the surface redox deposition favors the formation of a majority of bimetallic particles. Nevertheless, the presence of at least one large particle of

isolated Ru observed by TEM on this sample in Reference [25] reveals a limitation of the redox process which may occur for high modifier contents (higher to the value corresponding to a monolayer of Ru on Pt) resulting in the deposition of Ru agglomerates on the support by a simple impregnation. This limitation to deposit exclusively the additive on the metallic atoms of the parent catalyst was already observed in the case of Re–Pd/TiO_2 samples [27]. Thus, the Ru loading introduced by catalytic reduction deposition was decreased to prepare three new CR catalysts (entries 7 to 9). As expected, for a lower Ru loading (1 wt.%, entry 8), the TEM-EDX analysis indicates the absence of isolated Ru particles but mainly the presence of bimetallic particles with an average diameter of 3.8 nm and some small isolated Pt particles (Figure 1b).

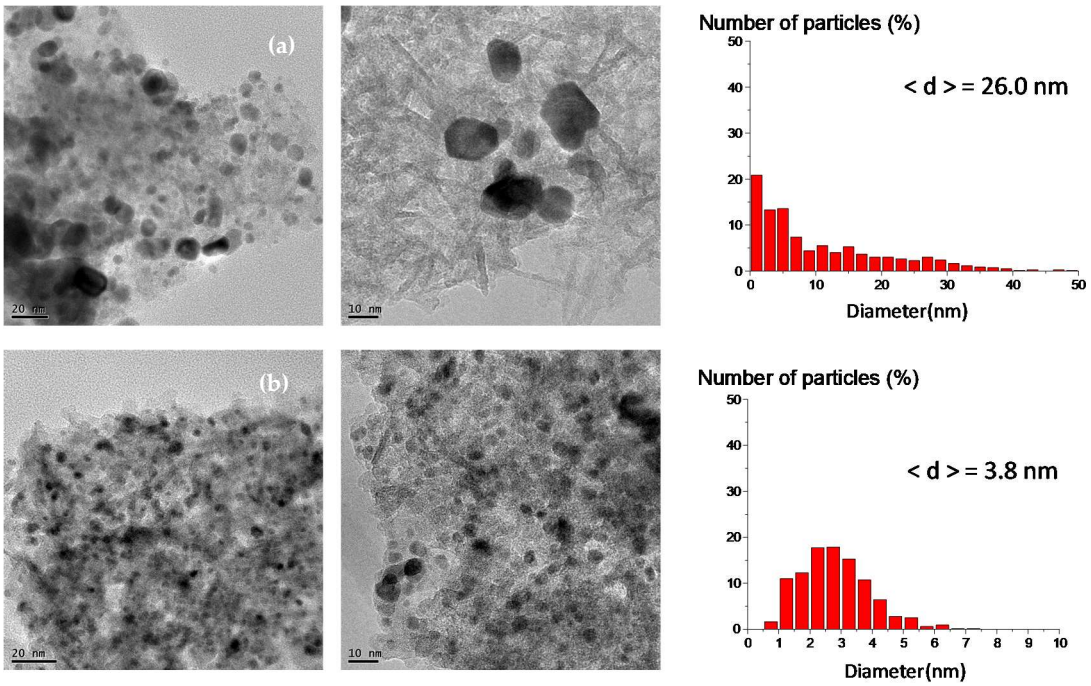

Figure 1. TEM pictures and size distribution of bimetallic catalysts: (**a**) SI–(Pt–Ru)/S40, (**b**) CR–(1%Ru–Pt)/S40. (TEM pictures representative of other bimetallic catalysts are available for consultation in Reference [25]).

XRD analyses were also performed in order to identify more precisely the nature of the metal phases present on the Ru–Pt bimetallic catalysts according to the preparation method. Figure 2 compares the diffractograms of the four bimetallic catalysts containing 3 wt.% Ru, with those of the S40 support, Ru/S40 and Pt/S40 monometallic catalysts. The XRD patterns of the Ru/S40, SI–(Pt–Ru)/S40 and CI–(Ru–Pt)/S40 samples reveal the presence of the Ru^0 phase that is not the case for the SI–(Ru–Pt)/S40 and CR–(Ru–Pt)/S40 catalysts. These results are in agreement with the TEM-EDX observations, where large particles consisting only of Ru atoms or very rich in Ru have been identified on both SI–(Pt–Ru)/S40 and CI systems, contrary to the SI–(Ru–Pt)/S40 and CR catalysts on which mainly small bimetallic particles have been identified [25]. The intensity of the diffraction peaks associated with Ru^0 varies according to the metal particles size of the catalysts. From the Debye-Scherrer formula, the sizes of Ru^0 particles are estimated to be about 10 nm, 15 nm and 17 nm for the Ru/S40, CI–(Ru–Pt)/S40 and SI–(Pt–Ru)/S40 samples, respectively, with some variations depending on the diffraction peak used for the calculation that may be due to heterogeneity in the size and shape of these particles. These values are smaller than the average diameters of the Ru-based particles deduced from TEM, namely 28 nm, 33 nm and 26 nm respectively. These discrepancies may result from an incomplete inventory of the smallest particles on the TEM images, leading to an increase

in the evaluation of their average diameter. Besides the γ-Al_2O_3 and Ru^0 phases, the other possible crystalline forms such as Pt^0 and/or PtRu alloy do not appear distinctly on the XRD patterns, probably due to the presence of too small particles size. Nevertheless, the presence of a PtRu alloy exhibiting a main diffraction peak at 40° can be assumed on the SI–(Ru–Pt)/S40 and CR–(Ru–Pt)/S40 catalysts that display diffractograms of comparable appearance and for which the three main diffraction peaks can be attributed to γ-Al_2O_3 and PtRu alloy phases [28,29].

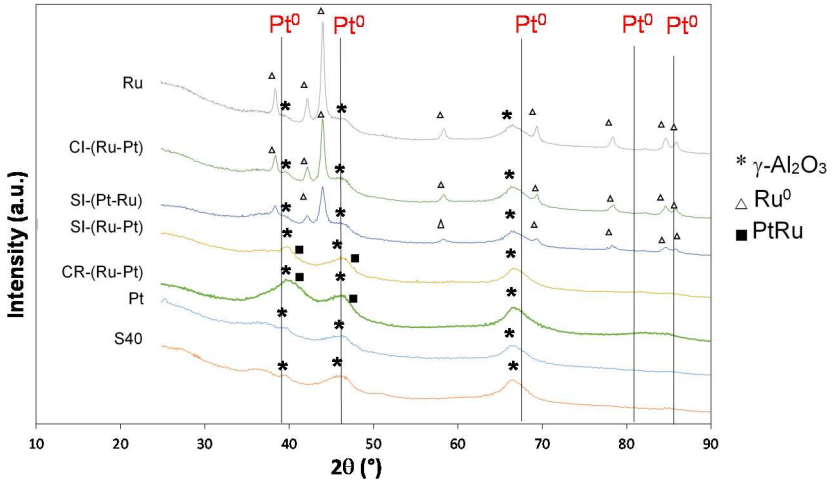

Figure 2. XRD patterns of the Ru–Pt/S40 bimetallic catalysts, according to their preparation method: co-impregnation (CI), successive impregnations (SI) or catalytic reduction deposition (CR) (the diffractograms of the lone support (S40), Pt/S40 and Ru/S40 monometallic catalysts are also given for comparison).

2.2. Chemical State of the Metal Function Determined by XPS

In order to better understand the chemical nature of the metal phases present on the surface of the synthesized catalysts, an XPS analysis was carried out on the CI–(Ru–Pt)/S40, SI–(Ru–Pt)/S40 and CR–(x%Ru-Pt)/S40 (x = 3 and 1 wt.%) bimetallic catalysts, as well as on the Pt and Ru monometallic systems, after an in-situ reduction at 450 °C under H_2. The decompositions of the spectra in the Pt 4f region given in Figure 3 show that the Pt 4f line emerges in the base of the peak associated with the Al 2p response. However, the Pt 4f line was preferred to the Pt 4d one due to the too weak response of this last (detection limit). For the study of the Ru chemical state, the decomposition was carried out from the Ru 3d profile (Figure 4), even if it was superimposed on that of the C 1s carbon, but the analyses remained nevertheless more accurate than with the Ru 3p band poorly definite [30,31]. Table 2 gathers all the results obtained after decomposition of the XPS spectra. It can be mentioned that on all activated samples the XPS analyses revealed no significant presence of chlorine species remaining after preparation with the chlorinated metal precursors and after HCl addition.

Figure 3 and Table 2 indicate that only Pt^0 species associated with a Pt 4f peak located at a binding energy (BE) of 71.1 ± 0.2 eV were detected on all samples, which is consistent with their totally reduced state after the reduction treatment confirmed by TPR experiments published in our previous work [25]. The study of the Ru 3d region (Figure 4 and Table 2) reveals that ruthenium was also exclusively in a Ru^0 state (BE = 279.3 ± 0.4 eV) for Ru/S40 and CI bimetallic catalysts, while Ru^{4+} species (probably associated to a RuO_2 phase, BE = 280.9 ± 0.3 eV) were identified on the three analyzed SI and CR bimetallic systems after reduction, with a proportion more or less equal to that of Ru^0. The presence of such oxidized Ru species after reduction was not demonstrated by XRD probably due to particles of too small size. Thus, the oxidation state of Ru appears directly linked to the nature of the Ru-based particles (totally isolated, or associated to Pt), and consequently to the preparation method of the bimetallic catalysts (CI, or SI and CR, respectively). It should be mentioned that a noticeable presence of carbon was found on these three bimetallic samples (C/Al atomic ratio

between 0.023 and 0.043), which can arise from the atmospheric CO_2 adsorbed on the solids during their storage and not eliminated during the in-situ reduction. In the case of the SI catalyst on which the detected C quantity was greatest, an oxidation treatment at 450 °C under pure O_2 was carried out in the pretreatment chamber of the XPS facility before the reduction at 450 °C, in order to best eliminate these carbon species (results corresponding to SI-(Ru-Pt)* in Table 2). This specific treatment before XPS analyses made dropping by more than half the carbon content detected on the sample (the C/Al ratio decreased from 0.043 to 0.020).

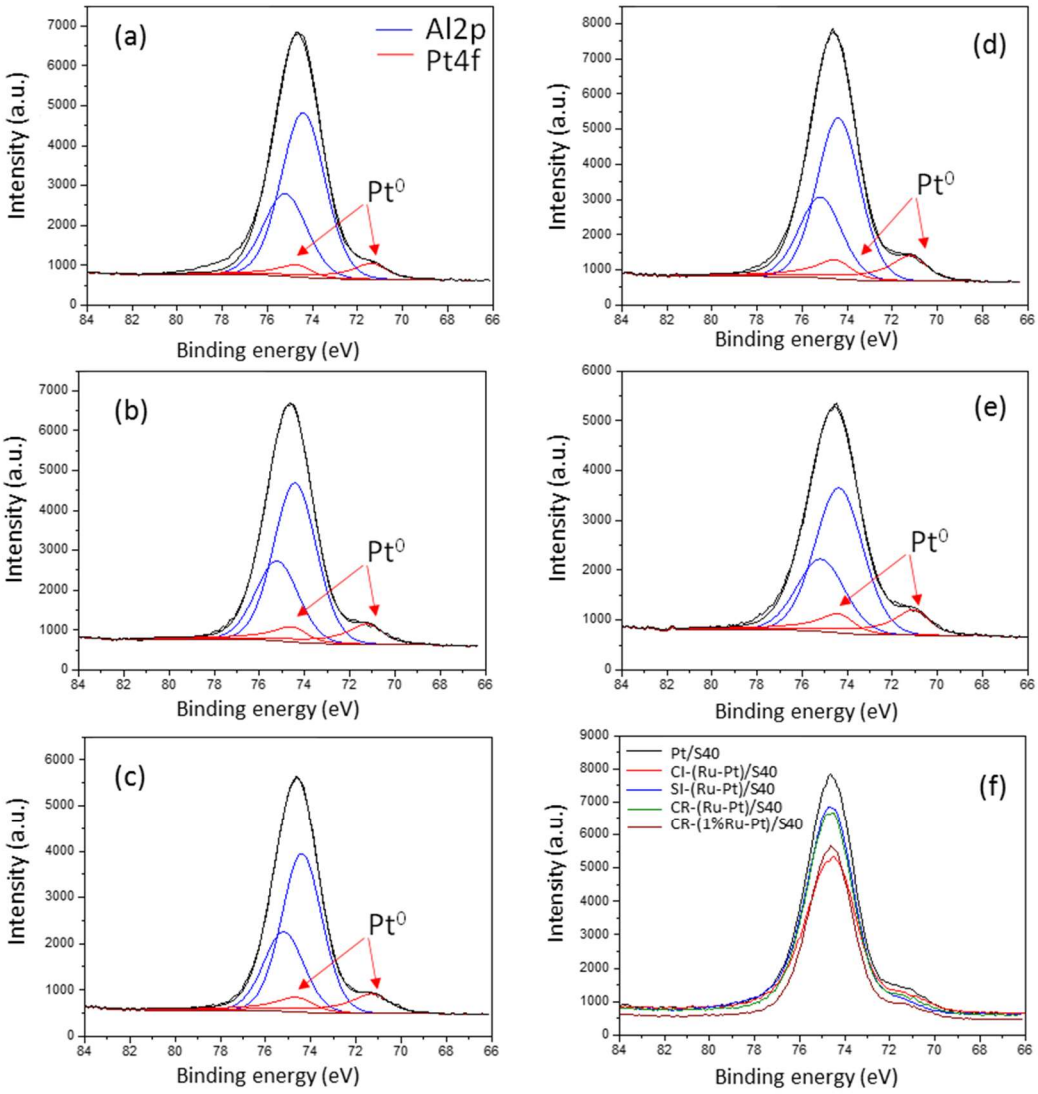

Figure 3. Curve fit of XPS data for Pt 4f region: (**a**) SI–(Ru–Pt)/S40, (**b**) CR–(Ru–Pt)/S40, (**c**) CR–(1%Ru–Pt)/S40, (**d**) Pt/S40, (**e**) CI–(Ru–Pt)/S40, (**f**) superposition of the Al 2p and Pt 4f bands for all samples.

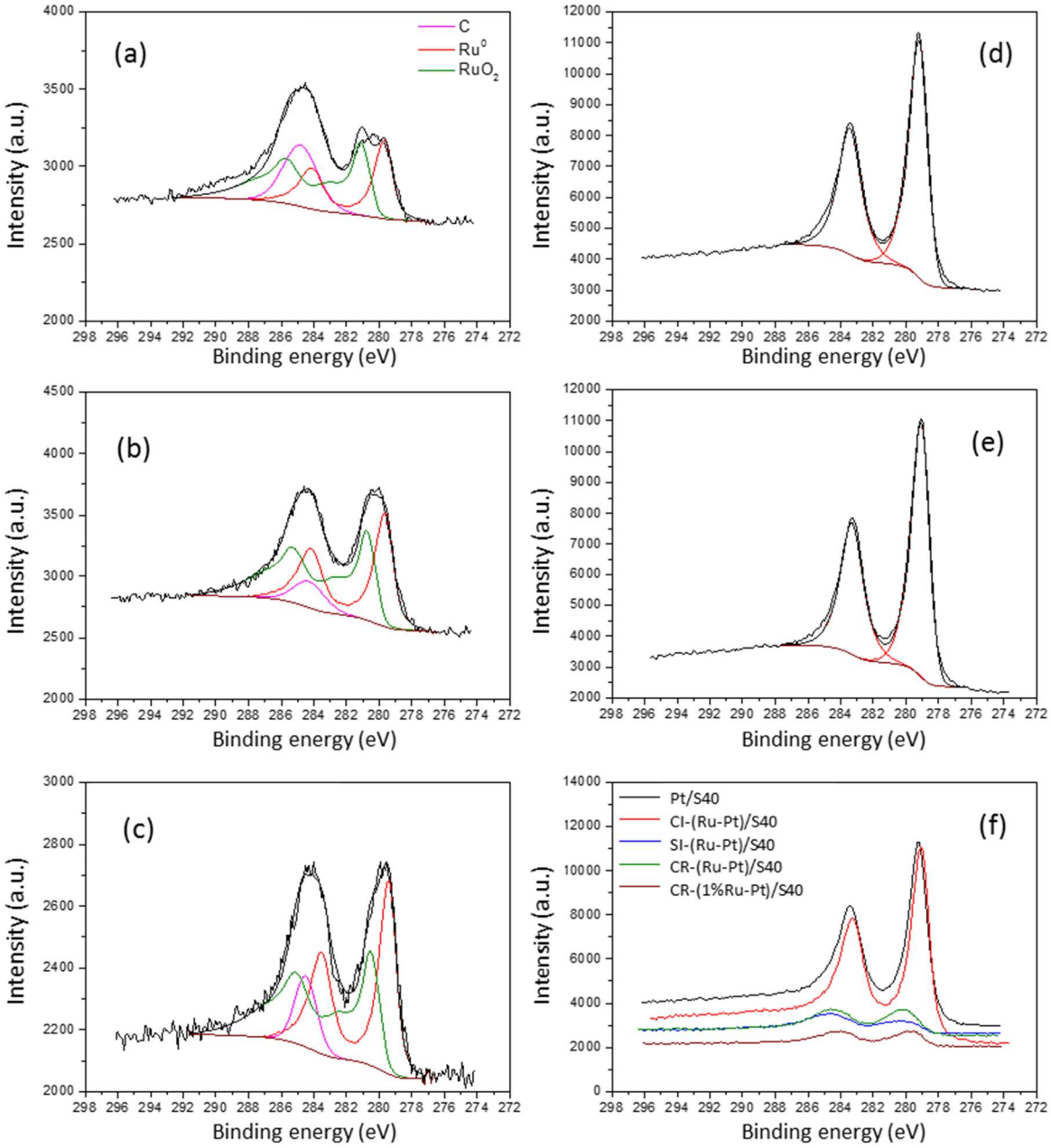

Figure 4. Curve fit of XPS data for Ru 3d region: (**a**) SI–(Ru–Pt)/S40, (**b**) CR–(Ru–Pt)/S40, (**c**) CR–(1%Ru–Pt)/S40, (**d**) Ru/S40, (**e**) CI–(Ru–Pt)/S40 (**f**) superposition of the Ru 3d band for all samples.

Table 2. XPS data of the Ru–Pt/S40 bimetallic catalysts prepared by co-impregnation (CI), successive impregnations (SI) or catalytic reduction deposition (CR), and of the corresponding monometallic samples: atomic percentages (%) and *binding energies* (*BE in eV*) of the Pt 4f and Ru 3d components and surface atomic ratios.

Catalysts/S40	Pt 4f	Ru 3d		Atomic ratio				
	Pt^0	Ru^0	Ru^{4+}	C/Al	Pt/Al	Ru/Al	Ru/Pt	$Ru^0/(Ru^0+Pt^0)$
Pt	100% *71.1*	-	-	-	0.010	-	-	-
Ru	-	100% *279.0*	-	-	-	0.050	-	-
CI-(Ru-Pt)	100% *71.0*	100% *278.9*	-	-	0.008	0.080	10.0	-
SI-(Ru-Pt)	100% *71.3*	44% *279.7*	56% *281.2*	0.043	0.005	0.009	1.8	0.44
SI-(Ru-Pt) *	100% *71.0*	80% *279.2*	20% *280.7*	0.020	0.005	0.012	2.5	0.67
CR-(Ru-Pt)	100% *71.1*	47% *279.7*	53% *280.8*	0.023	0.007	0.016	2.4	0.53
CR-(1%Ru-Pt)	100% *71.2*	50% *279.4*	50% *280.6*	0.024	0.008	0.012	1.5	0.43

* Catalyst oxidized in-situ at 450 °C under 5% O_2/Ar before the in-situ reduction.

On the three directly reduced SI and CR bimetallic catalysts, the BE of the Ru^0 peak shifts slightly to higher energies compared to the Ru monometallic and CI samples, suggesting the existence of an electronic transfer from ruthenium to platinum in accordance with the highest electronic affinity value for Pt. These observations are also consistent with the results of the model reaction of cyclohexane dehydrogenation displayed in Reference [25]. Indeed, on the SI and CR catalysts, an increase of the activity of the Pt sites was observed, the latter being the only ones able of converting cyclohexane to benzene in the studied experimental conditions. This increase was not consistent with the decrease in the number of accessible Pt atoms resulting from the Ru deposition, but can be explained by an electronic transfer from Ru towards Pt, reducing the interaction between the Pt sites and the benzene molecule and promoting, therefore, the desorption of this latter. Nevertheless, no significant impact was observed by XPS on the position of the Pt^0 peak on the concerned catalysts. The Pt amount detected by XPS analysis (300 × 700 μm probing area, depth of 10 nm) varies somewhat according to the catalysts but to a lesser extent compared to that of Ru: the Pt/Al atomic ratios evolve from 0.010 (Pt/S40) to 0.005 (SI–(Ru–Pt)/S40) and the Ru/Al ones from 0.050-0.080 (Ru/S40 and CI–(Ru–Pt)/S40) to 0.009–0.016 (SI and CR). For the catalysts containing 3 wt.% Pt and 3 wt.% Ru, the expected Pt/Al and Ru/Al atomic ratios are 0.013 and 0.025, respectively. The variations observed between the various experimental values can be related to the nature and the size of the particles that differ on the various samples. On the one hand, the Ru/S40 and bimetallic CI catalysts possess large ruthenium particles (Ru^0 form) in an isolated state with a respective average diameter of 28 nm and 33 nm, which can explain the higher Ru/Al atomic ratio on these two samples. From XPS analysis, the surface of the CI catalyst appears highly Ru enriched, the experimental Ru/Pt atomic ratio being 10.0 against a value of 1.9 calculated from the deposited metal contents. On the other hand, the SI and CR bimetallic catalysts (with 3 wt.% Ru as in the CI sample) exhibit bimetallic particles with homogeneous sizes and shapes with a respective average diameter of 2.3 and 2.6 nm, leading to a Ru/Pt ratio much closer to the expected value of 1.9 (1.8 and 2.4, respectively). The slight difference in particle size but also the presence of a large Ru particle isolated on the CR–(Ru–Pt)/S40 catalyst may explain that the Ru/Pt atomic ratio is higher on this sample. The CR–(1%Ru–Pt)/S40 bimetallic catalyst, containing less Ru atoms, leads logically to a lower Ru/Pt atomic ratio (1.5). Nevertheless, this ratio compared to the value deduced from the deposited contents (0.6) indicates the noticeable presence of Ru on the surface of this sample, which is in agreement with the principle of the catalytic reduction deposition involving a redox reaction on the surface of platinum particles.

Finally, the $\frac{Ru^0}{Ru^0+Pt^0}$ atomic ratio was calculated for the various SI and CR bimetallic catalysts, in order to estimate the alloyed PtRu phase composition that may be present while considering that the atomic quantities detected by XPS are representative of the set of these samples (which can be justified given the average particle size and the depth of the sample surveyed by the XPS analyses) [32]. Values between 0.43 and 0.53 were obtained for the three SI and CR catalysts after direct reduction, which remained consistent with the presumed presence of an alloy of PtRu formula on these catalysts. The treatment by oxidation and reducing before the analyses of the SI sample led to an increase of this ratio (0.67), indicating a Ru^0 enrichment within the bimetallic entities following the oxidation at high temperature [31]. It is obvious that the metal phase underwent restructuration during the oxidizing medium and was no longer representative of its real surface state [33]. For this reason, this treatment was not generalized to the other studied samples.

2.3. Characteristics of the Acidic Function

The total acidity of the bimetallic samples was measured by ammonia thermodesorption (NH_3-TPD) by integration of the TPD profiles between 100 and 450 °C (Figure S1). The sites associated with a strong acidity correspond to desorption temperatures between 360 and 450 °C. Moreover, the Brønsted acidity was evaluated by the catalytic activity for the isomerization reaction of 3,3-dimethylbut-1-ene (33DMB1). The 33DMB1 isomerization was carried out at 130 °C under atmospheric pressure in gaseous phase, it occurred through a pure protonic mechanism without the involvement of the Lewis centers, and led to the formation of only two products corresponding to the two isomers 2,3-dimethyl-1-butene and 2,3-dimethyl-2-butene [34–37]. The results of characterization of the acidic functions are gathered in Figure 5 for all studied samples.

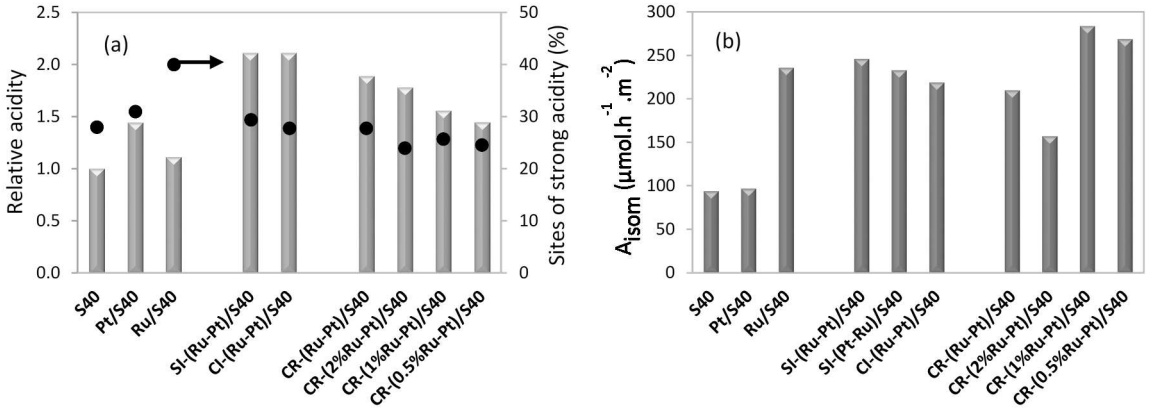

Figure 5. Acidic properties of the Ru–Pt/S40 bimetallic catalysts prepared by co-impregnation (CI), successive impregnations (SI) or catalytic reduction deposition (CR), and of the corresponding monometallic samples: (**a**) Relative total acidity measured by NH_3–TPD considering a total acidity of 1 µmol m^{-2} for S40 support, and the percentage of sites of strong acidity; (**b**) activity for isomerization of 33DMB1 at 130 °C.

The presence of Ru contributes to generate new Brønsted acid sites in addition to those present on S40 support, and/or to increase the strength of the existing sites, since the isomerizing activity increases significantly on all Ru-based catalysts compared to pristine S40 (Figure 5b). Except for the Ru monometallic catalyst which exhibits a higher percentage of strong acidity, this phenomenon is accompanied by a noticeable increase of the total acidity relative to S40 support; therefore, it is all the more important that the Ru content is high for the CR catalysts series (Figure 5a). In conclusion, compared to the Pt monometallic sample, all the bimetallic Ru–Pt catalysts display more numerous and/or stronger Brønsted acid sites, these sites being considered as those catalyzing dehydration reactions during the APHDO of polyols [16]. Some authors ascribed such an evolution of acidity to an increasing number of oxidized metal species on the surface [38,39]. Here the presence of Ru even in a

metallic state must influence the Brønsted acidity, since the monometallic Ru catalyst displaying no oxidized species according to the above XPS analyses, exhibits high activity for 33DMB1 isomerization.

2.4. Aqueous Phase Transformation of Sorbitol

Under similar conditions to those used in our previous paper [25] (batch reactor, 10 wt.% sorbitol aqueous solution, substrate/catalyst ratio of 15 w/w, 240 °C, 60 bar total pressure (H_2 atmosphere)), the bimetallic catalysts newly-synthesized in this work (SI–(Pt–Ru)/S40 and CR–(x%Ru-Pt)/S40) were tested for their sorbitol transformation into valuable hydrocarbons (i.e., C6, even C5). Figure 6 shows the global carbon distribution normalized to 100% obtained in the presence of the various studied systems at similar sorbitol conversions (between 80–96%), which corresponds to 1 or 2 h reaction time except for the CR–(0.5%Ru–Pt)/S40 bimetallic catalyst, which is slightly less active and achieves 80% conversion only after 3 h. During the sorbitol transformation, simultaneous C–O and C–C bond cleavages can occur leading to a variety of products found either in the gaseous phase (C1 to C6 hydrocarbons, and CO_2 issued from decarboxylation or decarbonylation followed by water gas shift reaction; no trace of CO was detected) or in the aqueous phase (oxygenated products, named oxygenates). Table 3 gathers the carbon yields in the liquid and gaseous phases obtained with the different catalysts, and the details of all the products identified in both phases are given in the supporting information (Tables S1 and S2).

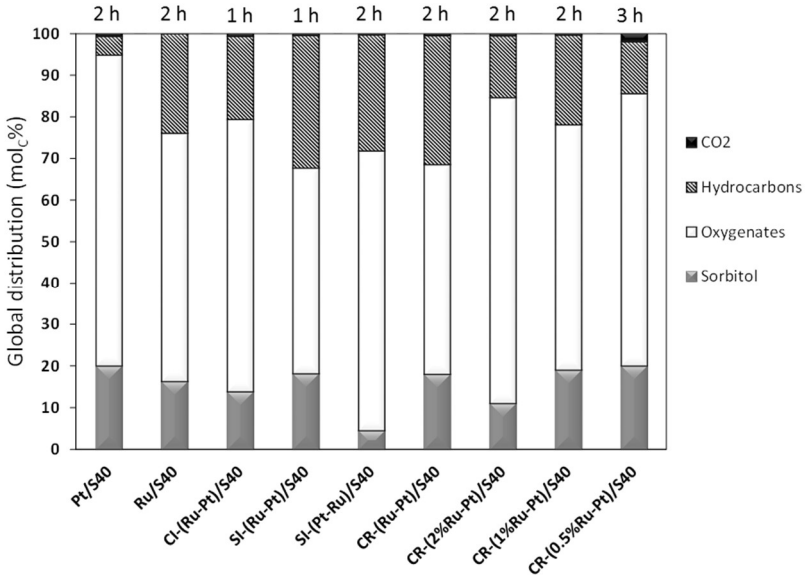

Figure 6. Carbon global distribution obtained at 80–96% sorbitol conversion for the Ru–Pt/S40 bimetallic catalysts prepared by co-impregnation (CI), successive impregnations (SI) and catalytic reduction deposition (CR), as well as for Pt and Ru monometallic catalysts.

The carbon balance systematically exceeds 80%, i.e., a value admitted as acceptable to correctly compare the performances of each catalyst (the volatility of some liquid compounds such as methanol may notably contribute to some carbon loss [40]). For all samples, most of the carbon is in the liquid phase in the form of oxygenated products. With catalysts containing Ru, C1 to C5 oxygenated compounds were observed while they were few present with the Pt/S40 catalyst. The C3–C5 compounds correspond mainly to polyols (glycerol, propanediols, erythritol, and xylitol) and C1 to methanol. Especially, the formation of C3 oxygenated compounds was observed particularly in the presence of CR catalysts. They are generally assumed to be formed by C–C hydrogenolysis on the metal function or retro-aldolisation [41–44].

Table 3. Carbon yields in aqueous and gaseous phases obtained at 80–96% sorbitol conversion for the Ru–Pt/S40 bimetallic catalysts prepared by co-impregnation (CI), successive impregnations (SI) and catalytic reduction deposition (CR), as well as for Pt/S40 and Ru/S40 monometallic catalysts.

Catalysts/S40	C_{liq} [1] ($\%_{carbon}$)	Identification Ratio [2]	C_{gas} [3] ($\%_{carbon}$)	C_{hexane} ($\%_{carbon}$)
Pt	74.9	1.00	5.5	3.7
Ru	59.8	1.00	23.9	9.6
CI-(Ru-Pt)	65.6	0.90	20.6	2.4
SI-(Ru-Pt)	49.5	1.00	32.3	24.4
SI-(Pt-Ru)	67.3	1.00	28.2	2.3
CR-(Ru-Pt)	49.9	0.95	31.6	1.8
CR-(2%Ru-Pt)	73.6	1.00	15.4	1.9
CR-(1%Ru-Pt)	59.1	1.00	21.8	11.4
CR-(0.5%Ru-Pt)	65.6	1.00	14.4	8.2

[1] [(Carbon detected in formed liquid products)/(Carbon in the feed solution)] × 100. [2] Identification ratio = Σ(carbon concentration identified in the liquid phase)/TOC. With TOC = Total Organic Carbon in the liquid phase. [3] [(Carbon detected in formed gaseous products)/(Carbon in the feed solution)] × 100.

All bimetallic catalysts lead to a higher proportion of hydrocarbons than the Pt/S40 monometallic catalyst. However, only the two SI catalysts and the CR sample with the highest Ru load (CR-(Ru-Pt)/S40) display a higher proportion of hydrocarbons than the Ru/S40 monometallic catalyst, i.e., around 31 mol_C% compared to around 24 mol_C%. In the CR series, the hydrocarbons proportion seems to increase with the Ru content, with a particular behavior for the CR–(2%Ru–Pt)/S40 catalyst for which the carbon amount in the gas phase is surprisingly the lowest. This atypical behavior could be related to the lower isomerizing activity observed with this sample within the CR series (Figure 5b), and thus, to the presence of less numerous or less effective Brønsted acid sites to ensure the cleavage of C–O bonds of sorbitol and oxygenated intermediates, which are necessary to form hydrocarbons. With the new bimetallic samples, SI–(Pt–Ru)/S40 and CR–(2%Ru–Pt)/S40, the proportion of methane prevails over that of hexane, as it was the case for the CI and CR (with 3 wt.% Ru) samples previously prepared. This tendency was explained by the high capacity of Ru to cleave the C–C bond [45,46]. By using the CR preparation method, the proportion of methane tends to decrease with the decreasing ruthenium load, and inversely the formation of hexane increases. Effectively, in contrast to the CR–(Ru–Pt)/S40 and CR–(2%Ru–Pt)/S40 catalysts, the CR–(1%Ru–Pt)/S40 and CR–(0.5%Ru–Pt)/S40 systems lead to a higher proportion of hexane than of methane in the gas phase. The CR bimetallic catalyst loaded with 1 wt.% Ru corresponds finally to the best catalyst of the series in terms of hexane selectivity, due undoubtedly to a better balance between acidic function and metallic function on this sample possessing the highest isomerizing activity of the series (Figure 5b). In the end, the CR–(1%Ru–Pt)/S40 and SI–(Ru–Pt)/S40 catalysts are the only two bimetallic systems that allow increasing the amount of hexane formed compared to the Pt/S40 and Ru/S40 samples. This increase remains truly remarkable in the case of the SI catalyst, with a higher hexane yield of 24 mol_C% at about 80% sorbitol conversion. These catalysts are the only two catalytic systems that have bimetallic particles of fairly homogeneous and small sizes (đ = 3.8 and 2.3 nm for CR and SI systems, respectively). On these two samples, the Pt and Ru species are therefore in strong interaction, the presence of a PtRu type alloy being highly suspected according to the XRD and XPS analyses. However, it can be supposed that the presence of a PtRu alloy is not compulsory to explain the synergistic catalytic activity as already reported by Antolini et al. [47]. Nevertheless, here the essential role of the Pt–Ru bimetallic interaction seems undeniable in explaining the evolutions of the catalytic performances in terms of hexane yield, since the CI system possessing two distinct Pt and Ru phases proves to be ineffective. The intervention of oxidized Ru species (Ru^{4+}) identified by XPS on the surface of the two concerned SI and CR samples can also contribute to explain the observed synergistic phenomenon, moreover these species are more numerous on the most efficient system i.e., the SI catalyst (Table 2).

The SI–(Ru–Pt)/S40 and CR–(Ru–Pt)/S40 bimetallic catalysts, as well as the Pt/S40 sample, were characterized at the end of the sorbitol conversion test, i.e., after 6 h reaction time. These two bimetallic samples were selected because they both displayed particles of small and homogeneous sizes in their fresh state. Figure 7 shows examples of TEM images and particle size distributions obtained for these "used" catalysts, and Table 4 gives the main characteristics of the three catalysts in the used state (to compare with values given in Table 1 for the fresh samples).

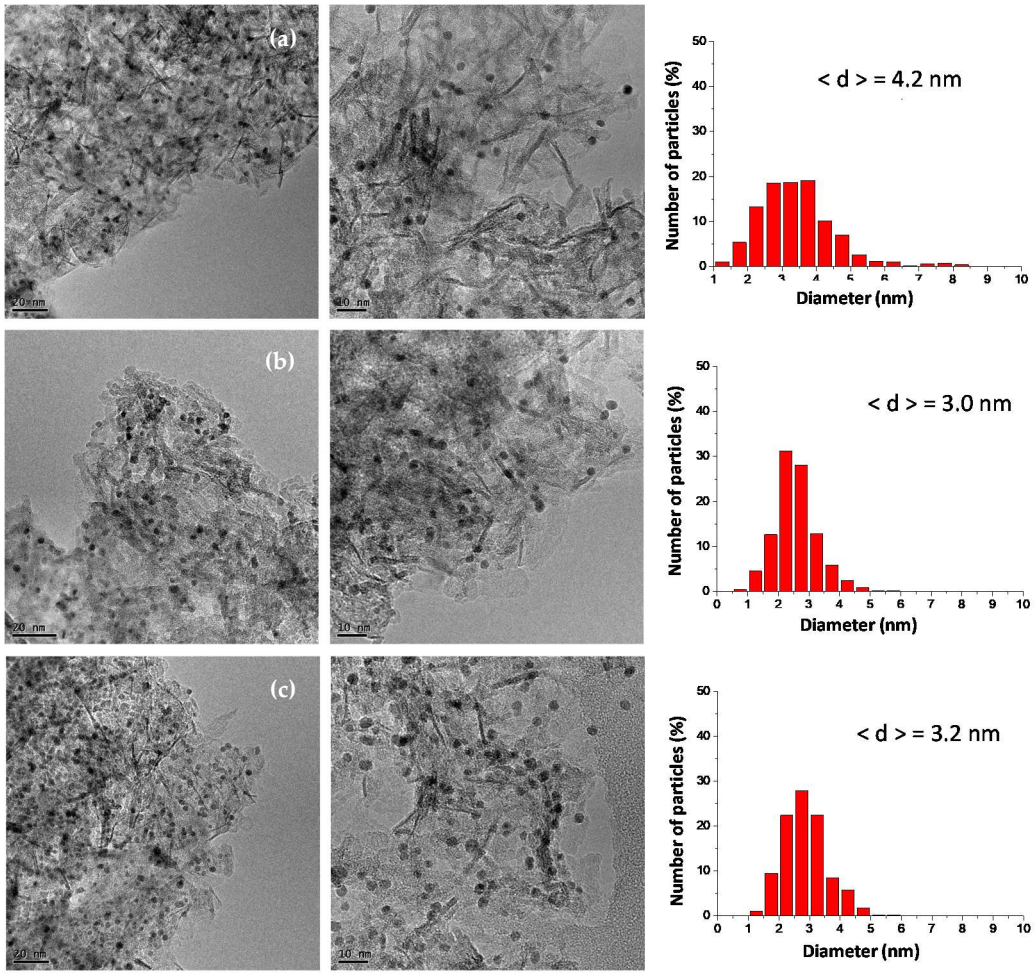

Figure 7. TEM images of catalysts after the test of sorbitol transformation: (**a**) used Pt/S40, (**b**) used SI–(Ru–Pt)/S40, (**c**) used CR–Ru–Pt)/S40.

Table 4. Characteristics of the SI–(Ru–Pt)/S40 and CR–(Ru–Pt)/S40 bimetallic catalysts, as well as the Pt/S40 sample, after the catalytic test of sorbitol transformation.

Catalysts/S40	S_{BET} [1] ($m^2\ g^{-1}$)	V_P [1] ($cm^3\ g^{-1}$)	D_P [1] (nm)	d [2] (nm)	Carbon [3] (wt.%)	Hydrogen [3] (wt.%)
Pt used	367	0.77	7.1	4.2	22.6	3.8
SI–(Ru–Pt) used	313	0.72	8.2	3.0	16.3	2.5
CR–(Ru–Pt) used	395	0.83	7.9	3.2	4.0	1.5

[1] Specific surface area S_{BET}, pore volume V_P and pore diameter D_P determined by N_2 sorption measurements. [2] Average particles size determined by TEM analysis. [3] Weight contents determined by elemental analysis of the used catalysts after 6 h sorbitol transformation.

A sintering of the metal particles was observed after the catalytic test, which is in agreement with the results reported in the literature for reactions performed under similar hydrothermal conditions [48,49]. This sintering is of a lesser amplitude in the case of the bimetallic formulations.

Indeed, the average sizes evolve from 2.3 to 3.0 nm and from 2.6 to 3.2 nm for the SI and CR systems, respectively, against an evolution of 1.1 to 4.2 nm for the Pt/S40 system. However, the metal particles remained fairly well dispersed on the support. The elemental analysis of the used samples given in Table 4 indicates the presence of carbon on their surface. The used Pt/S40 sample was composed of 22.6 wt.% carbon, which represents about 4% of the carbon provided by the sorbitol feedstock introduced in the batch reactor. Carbon deposition is caused by the accumulation on the catalyst surface of oxygenated hydrocarbons with high boiling points (> 120 °C, i.e., the drying temperature applied to the catalytic sample once recovered after test). Nevertheless, the carbonaceous deposition is less important on the bimetallic catalysts than on the Pt/S40 system, and in particular on the CR one. At least two hypotheses can be advanced to explain this tendency: (i) the chemical nature of the oxygenated intermediates generating the carbon deposition differs between the monometallic and bimetallic catalysts, and (ii) the carbon deposition on acidic sites can be suppressed by the Pt–Ru interaction due to an increase of the hydrogen spillover as previously observed with supported Pt–Re catalysts [19,50]. Table 4 also indicates some changes in the textural properties of the catalysts after the catalytic test with an increase of the surface area in the case of bimetallic catalysts. Moreover, the analysis by ICP-OES of the liquid effluent recovered at the end of the catalytic test revealed no trace of Pt and Ru, i.e., the absence of metal leaching in the solution. The pH of the aqueous solution of sorbitol, initially around 5.5, was observed to decrease after the test until a value in the range of 3–4. The formation of acidic intermediate compounds is generally referred to, to explain this evolution of pH [49].

2.5. Reactivity of Intermediate Species

In order to better understand the different catalytic behaviors of the various Ru–Pt bimetallic systems, it is important to compare in more depth the composition of the liquid phase during the transformation of sorbitol (Tables S1 and S2 give the composition at 80–96% of sorbitol conversion for all studied catalysts). In agreement with previous studies relating to the nature of main intermediates during the aqueous-phase hydrodeoxygenation of sorbitol [15,16,19,51], the aqueous phase was composed mainly of C6 oxygenated compounds for all studied catalysts, with the majority corresponding to sorbitan and isosorbide (mono- and bi-cyclic polyols obtained after one and two dehydrations of sorbitol, respectively); 1,2,6-hexanetriol; 1,2-hexanediol; hexanol; and some cyclic ether compounds (tetrahydropyran-2-methanol, 2-methyl-tetrahydropyran, 2,5-dimethylfuran, 2,5-dimethyltetrahydrofuran). In Reference [25], we observed a noticeable formation of the furanic intermediates during the first hour of reaction with the Ru-based catalysts compared to Pt/S40, and notably with the SI–(Ru–Pt)/S40 sample displaying the highest hexane yield. Likewise, these compounds are formed in noticeable quantity at the beginning of the reaction in the presence of the CR–(1%Ru–Pt)/S40 catalyst, the highest selective to hexane of the CR series. Indeed, with this catalyst around 6 mol_C% are attributed to furanic compounds after 1 h of reaction. Consequently, complementary experiments were undertaken to compare the reactivity of two C6 intermediate oxygenated products, namely isosorbide and 2,5-dimethylfuran (2,5-DMF). Only the SI–(Ru–Pt)/S40 bimetallic sample was used to conduct these complementary experiments since it was observed as the most efficient of the studied catalysts to selectively convert sorbitol to liquid alkanes. The experimental conditions were similar to those used for hydrothermal sorbitol transformation: 1 g of catalyst, 240 °C, pressure of 60 bar (H_2 atmosphere), and an initial charge of substrate adjusted to correspond to the carbon amount present in the autoclave during the sorbitol transformation if this latter (15 g) is totally converted to this substrate (i.e., an aqueous solution of 8 and 5 wt.% for isosorbide and 2,5-DMF, respectively).

Figure 8a shows the evolution of the isosorbide conversion as a function of time on the Pt/S40 and SI–(Ru–Pt)/S40 catalysts. The monometallic catalyst is significantly less active than the bimetallic one, the conversion reaching a maximum of only 40% in the first case against 88% in the second case at the end of the reaction. Thus, on both catalysts, isosorbide is not completely converted after 6 h reaction

time in agreement with the above results obtained during the transformation of sorbitol. Moreover, the isosorbide reactivity appears to be less than that of sorbitol, since when sorbitol was used as a substrate on these same catalysts, it was completely converted after 3 h of reaction. Knowing that during sorbitol transformation, the isosorbide conversion is certainly limited as long as sorbitol remains in the solution, these results are consistent with the fact that over a period of 6 h of reaction the liquid phase is mainly constituted of this intermediate compound, especially with the monometallic Pt/S40 being less efficient to convert it. The overall distribution of carbon obtained at about 40% conversion of isosorbide with the monometallic and bimetallic catalysts (i.e., at 6 h and 1 h reaction time, respectively) and at the end of the reaction (6 h) with the SI sample is given on Figure 8b. At 40% isosorbide conversion, the products formed in the presence of the monometallic catalyst are predominantly oxygenated compounds in the liquid phase while those in the gas phase dominate with the bimetallic catalyst. Thus, the hydrocarbon yields are equal to 23.9 mol_C% with the SI–(Ru–Pt)/S40 sample against only 10.1 mol_C% with the Pt/S40 one, and after the same reaction time (6 h), this yield reaches 58.8 mol_C% with this first. As during the sorbitol transformation, a very small quantity of CO_2 is formed at 40% conversion (< 0.5 mol_C%), however, with an increase of up to 6.6 mol_C% on the SI sample at the end of the reaction.

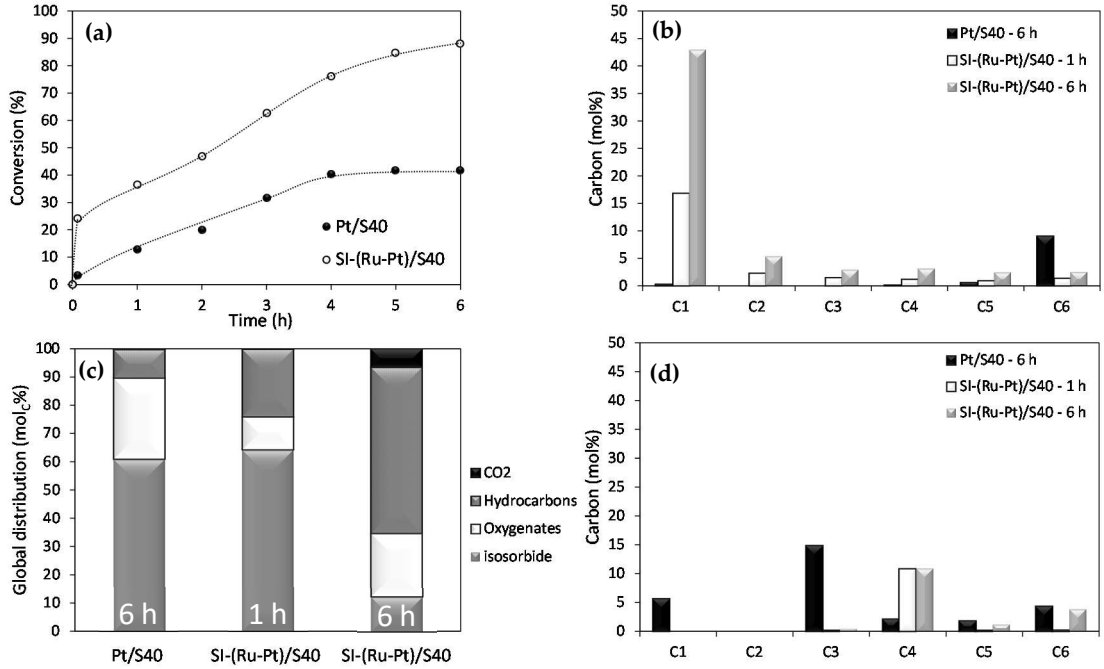

Figure 8. Comparison of the performances of the SI–(Ru–Pt)/S40 bimetallic catalyst and the Pt/S40 monometallic catalyst for isosorbide transformation: (**a**) conversion as function of time, (**b**) carbon distribution in the gas phase at the indicated reaction time, (**c**) carbon global distribution obtained at the indicated reaction time and (**d**) carbon distribution in the liquid phase at the indicated reaction time.

Figure 8c,d show the carbon distribution in the gas and liquid phases, respectively, obtained with the two catalysts (the C1 compound in the gas phase corresponding mostly to methane). While on the monometallic Pt/S40 catalyst, hexane represents 90% of the hydrocarbons formed, a similar proportion to that observed starting from sorbitol; the bimetallic SI–(Ru–Pt)/S40 sample induces C–C bond cleavages with the formation in majority of methane, namely 16.9 mol_C% and 43.0 mol_C% at 1 and 6 h reaction time, respectively (i.e., about 70% of hydrocarbons formed in both cases). This behavior is hardly comparable to the results obtained on this catalyst with sorbitol as the substrate, since hexane was then the main hydrocarbon in the gas phase. In the liquid phase, the monometallic catalyst leads to the formation of the following oxygenated compounds classified by decreasing quantity: C3 (propanediols and propanols), C1 (methanol), C6 (1,2,6-hexanetriol, 1,2-hexanediol, hexanols,

sorbitan), C4 (erythritol) and finally C5 (2-methyltetrahydrofuran, 1,2-pentanediol, pentanols). At isoconversion, the bimetallic catalyst forms mainly erythritol (C4), and after 6 h reaction time, C5 (2-methyltetrahydrofuran and 1,2-pentanediol) and C6 compounds (2,5-dimethyltetrahydrofuran) are detected. To resume, with the Pt/S40 catalyst, the isosorbide transformation induces the formation of oxygenated compounds originating mainly from C–C bond cleavages, the compounds are then negligible with sorbitol as the substrate. And with the SI bimetallic system, the C–C bond cleavage reactions are also important, leading to a massive formation of methane typical of the hydrogenolytic character of ruthenium [45,46]. These results tend to prove that during the transformation of sorbitol: (i) the isosorbide intermediate predominantly formed on the Pt/S40 system has a lower reactivity in the presence of sorbitol in agreement with the observations of Op de Beeck et al. [52]; (ii) starting from sorbitol as the substrate, the SI–(Ru–Pt)/S40 bimetallic catalyst follows a reaction mechanism to form hexane not predominantly involving the isosorbide intermediate.

The transformation of 2,5-DMF was further carried out on the SI–(Ru–Pt)/S40 catalyst under the same hydrothermal conditions with an initial charge of 5 wt.% in aqueous solution. As shown in Figure 9 describing the overall carbon distribution as a function of time, unlike sorbitol and isosorbide, the 2,5-DMF conversion reaches 99% after 5 min of reaction. After this reaction time, the compound predominantly present in the liquid phase is 2,5-dimethyltetrahydrofuran (2,5-DMTHF) resulting from the hydrogenation of the substrate. The hydrogenation of 2,5-DMF to 2,5-DMTHF is very rapid, and the conversion of this latter also since, after 1 h of reaction, the oxygenated compounds in the liquid phase become very minor, and rapidly the majority of the carbon is concentrated in the gas phase and mainly as hexane (89 mol_C%). Therefore, 2,5-DMF, as well as 2,5-DMTHF, are oxygenated compounds more reactive than isosorbide, and their conversion on the SI bimetallic catalyst induces very few C–C bond cleavages (few C1-C5 products detected), leading to a high selectivity to hexane. Starting from sorbitol (or isosorbide), the SI–(Ru–Pt)/S40 system has generated more C1–C5 byproducts due to the competition between the two following major sorbitol transformation pathways:

- pathway (1):

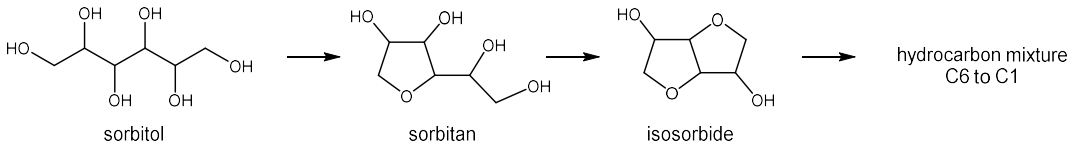

- pathway (2):

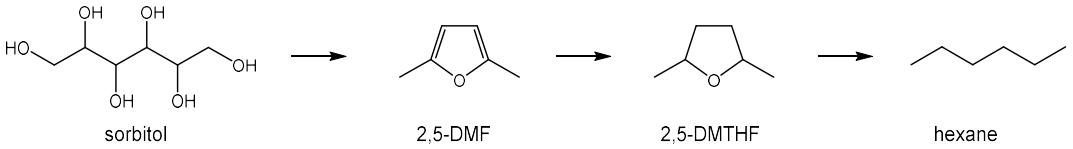

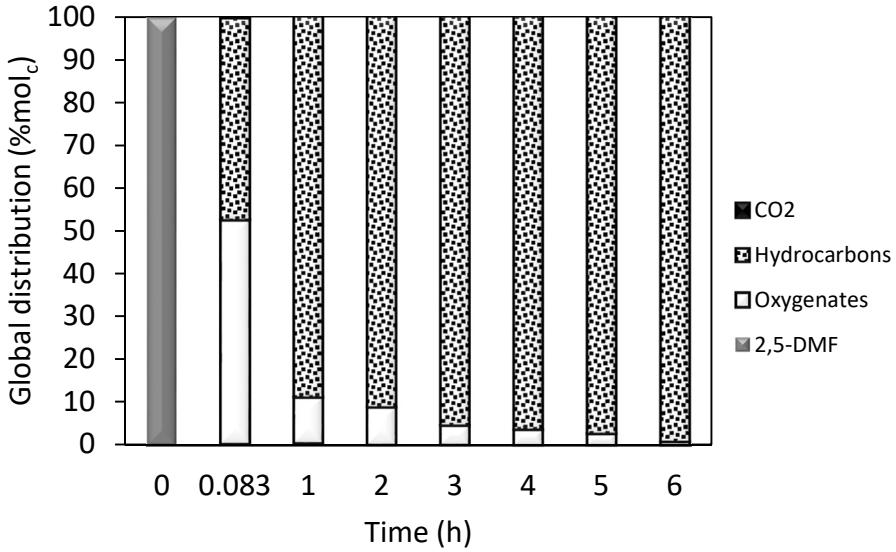

Figure 9. Carbon global distribution as a function of time during the 2,5-dimethylfuran (2,5-DMF) transformation on the SI–(Ru–Pt)/S40 bimetallic catalyst.

The pathway (2) appears as the preferred route for selectively obtaining hexane. In their study related to the direct conversion of cellulose to alkanes on ruthenium-based monometallic catalyst supported on carbon and modified with tungstosilicic acid ($H_4SiW_{12}O_{40}$), Op de Beeck et al. [52] also found that furanic compounds such as 2,5-DMF are much more reactive than isosorbide for obtaining pentane and hexane. Indeed, by comparing the transformations of the three substrates, i.e., sorbitol, isosorbide and 2,5-DMTHF, the authors observed very different yields of hexane, respectively, 4.3 mol_C%, 8.7 mol_C% and 82.9 mol_C%. Thus, concerning the Ru–Pt catalysts studied in the present work, the successive impregnations of first the Pt salt and further the Ru one (SI–(Ru–Pt)/S40 catalyst), as well as to a lesser extent, the deposition of Ru salt by catalytic reduction on the Pt/S40 catalyst (CR-(1%Ru-Pt)/S40 catalyst), allow synthesizing bimetallic systems active for the both reaction pathways during the sorbitol transformation, thus leading to the best hexane formation among all the studied catalysts. Arguments often advanced to explain the effect of the promoter in bimetallic catalysts are a reduction of the adsorption enthalpy of hydrogen and CO on the metal surface, promoting the desorption of these products and then leaving more sites accessible for the reaction [53], or the chemisorption of hydroxyl groups by certain co-metals (such as Re) to form alkoxides that can catalyze C–O bond cleavages by dehydration reactions or even direct hydrogenolysis in some cases [38,54]. In our study, we consider that the Pt modification by Ru via SI and CR methods favors a more selective formation of 2,5-DMF, intermediate kinetically more reactive than isosorbide and selectively convertible to hexane.

3. Materials and Methods

3.1. Catalysts Preparation

The silica–alumina from Sasol (SIRAL 40 noted S40, 60 wt.% Al_2O_3 and 40 wt.% SiO_2) used as support displayed the following textural characteristics: a specific surface area of 510 $m^2\ g^{-1}$, a pore volume of 0.9 $cm^3\ g^{-1}$ and an average pore diameter of 9.0 nm. A treatment by calcination under air at 500 °C for 4 h (10 °C min^{-1} and 60 $cm^3\ min^{-1}$) was applied to the support before its impregnation by metal precursor salts, i.e., hexachloroplatinic acid (H_2PtCl_6 from Sigma-Aldrich, 37.5 wt.% Pt, Saint-Quentin Fallavier, France) and ruthenium trichloride ($RuCl_3$ from Sigma-Aldrich, 45.0 wt.% Ru, Saint-Quentin Fallavier, France) in aqueous solutions at pH 1 (controlled by HCl addition). Several Ru–Pt/SiO_2–Al_2O_3 bimetallic catalysts were prepared either by classical co-impregnation (CI), successive impregnations (SI) or catalytic reduction deposition (CR), according to experimental

protocols described in detail in a previous paper [25]. For the SI and CR catalysts, the preparation started with the synthesis of a monometallic sample (Pt/S40 or Ru/S40) before the second impregnation (SI) or the catalytic reduction deposition (CR) of the second precursor salt. The metal compositions of the prepared bimetallic catalysts were adjusted to obtain: (i) for CI and SI samples, 3 wt.% of Pt and 3 wt.% of Ru and (ii) for CR samples, 3 wt.% of Pt and x wt.% of Ru. The various catalysts will be represented as follows: CI–(Ru–Pt)/S40; SI–(Ru–Pt)/S40 for which Pt salt was the first impregnated one; SI–(Pt–Ru)/S40 for which the Ru salt was the first impregnated one; and CR-(x%Ru-Pt)/S40 for which a Pt/S40 catalyst was used as a parent sample activating the hydrogen involved in the catalytic reduction process of Ru salt (the Ru content deposited being variable: x = 0.5, 1, 2 or 3 wt.%). At the end of their preparation, the bimetallic catalysts were activated according to the following treatments: (i) the CI sample was calcined at 350 °C for 2 h under air flow (10 °C min^{-1}, 60 cm^3 min^{-1}) and reduced at 450 °C for 3 h under H_2 flow (10 °C min^{-1}, 60 cm^3 min^{-1}); (ii) for the SI and CR methods, firstly, the monometallic catalyst was calcined at 450 °C (Pt/S40) or 350 °C (Ru/S40) for 2 h under flowing air (10 °C min^{-1}, 60 cm^3 min^{-1}) and reduced at 400 °C (Pt/S40) or 500 °C (Ru/S40) for 2 h under flowing H_2 (10 °C min^{-1}, 60 cm^3 min^{-1}); and secondly, the bimetallic catalysts were reduced under H_2 flow (60 cm^3 min^{-1}) at 450 °C for 3 h.

The analyses of the weight loadings on the catalysts, performed by optical emission spectrometry using inductively coupled plasma (ICP-OES) or atomic absorption, confirmed that the metal contents really deposited on the support are quite comparable to the expected ones taking into account the measurement uncertainty (i.e., a relative error estimated to 7%).

3.2. Characterization of the Catalysts

The physical and textural properties of the catalysts, i.e., the specific surface area (S_{BET}), the pore size distribution (D_p) and the pore volume (V_p), were determined by physisorption of nitrogen at −196 °C on a TRISTAR Micromeritics apparatus according to the procedure described in a previous paper [25].

The morphology of the catalysts was evaluated by transmission electron microscopy (TEM) using a JEOL 2100 instrument (JEOL Europe SAS, Croissy Sur Seine, France) coupled with energy dispersive X-ray spectroscopy (EDXS), in order to observe the accurate localization of the metallic particles, to analyse their chemical nature and to estimate their average size. The preparation of the samples and the experimental conditions were the same as in our previous paper [25]. The average particle size of a sample was determined by measuring with the ImageJ software at least 300 particles, from at least five different micrographs, and using the following formula: $\bar{d} = \Sigma n_i d_i^3 / \Sigma n_i d_i^2$ (d_i = diameter of n_i particles).

X-ray diffraction (XRD) experiments (Malvern Panalytical SARL, Orsay, France) were performed in order to determine the crystalline structure of the catalysts, according to the following conditions: EMPYREAN apparatus (PANanalytical) using Cu K_α radiation (λ = 0.154245 nm) as X-ray source, operating at 45 kV and 40 mA; diffractograms collected for 2λ from 15° to 90° with a step of 0.08° (acquisition time of 600 s); identification of the crystalline phases by means of the HighScore Plus software (version 3.0d(3.0.4), Malvern Panalytical SARL, Orsay, France) and the ICDD database.

The surface chemical composition and oxidation states of Pt and Ru in catalyst samples were analyzed by X-ray photoelectron spectroscopy (XPS) using a hemispherical analyzer on a Kratos Axis Ultra ^{DLD} spectrometer with a delay line detector and charge neutralization system (Kratos Analytical Ltd., Manchester, United Kingdom). XPS spectra were collected with a monochromated Al K_α X-ray source (hν = 1486.6 eV) operating at 150 W, 15 kV and 10 mA. In-situ pretreatment of the solids at 450 °C in H_2 atmosphere (5 °C min^{-1}, 1 h) was performed in a cell directly connected to the XPS chamber. After pretreatment, the samples were cooled to room temperature and transferred without exposure to air into the ultra-high vacuum chamber (10^{-9} mbar). Peak fitting was achieved using CASA XPS software. Quantitative determinations were performed using the Vision KRATOS software.

The Pt 4f and Ru 3d components were used for determining the binding energy (BE) and the chemical state of the samples, the BEs being referenced to the Al 2p line at 74.4 eV.

The total amount of acidic sites and the Brønsted acidity of the catalysts were evaluated by ammonia temperature-programmed desorption (NH_3-TPD) on an Autochem II 2920 apparatus (from Micromeritics France S.A.R.L., Merignac, France) and by the model reaction of skeletal isomerization of 3,3-dimethyl-1-butene (33DMB1), respectively. Both experiments were performed on catalysts reactivated in-situ under hydrogen according to the procedures described in details in our previous work [55].

3.3. Aqueous-phase Transformation of Sorbitol

A 300-mL stainless steel reactor (Autoclave Engineers Europe, Wexford, Republic of Ireland) fitted with systems for liquid and gas sampling was used for the catalytic test of sorbitol transformation in the aqueous phase. In brief, the experimental conditions are the following: 1 g of pre-reduced catalyst; a 10 wt.% aqueous solution of sorbitol (150 cm^3 of water with 15 g of sorbitol); substrate/catalyst ratio of 15 w/w; constant temperature of 240 °C; constant pressure of 60 bar (hydrogen atmosphere); 1300 rpm of stirring (the zero time being fixed when the stirring was switched on once the temperature and pressure reached their expected values). At different reaction times, gaseous products were analyzed on-line with a CP-2800 RGA chromatograph equipped with an injection valve and three detection channels (2 TCD and 1 FID), and liquid samples (manually collected) by HPLC (from Shimadzu France, Noisiel, France), by using sulphuric acid in water as a mobile phase (0.004 mol L^{-1}, 0.5 mL min^{-1}), a BIO-RAD Aminex HPX 87H column kept at 30 °C, and both refractive index (RI) and ultraviolet (UV) detectors. The total quantity of carbon in the aqueous phase was also measured by total organic carbon (TOC) analysis with a Shimadzu apparatus (Carbon-L Series). Sorbitol conversion, yields in liquid and gas phase (C_{liq} and C_{gas}) expressed in carbon molar percentage ($\%mol_C$) were calculated on the basis of the following equations:

$$\text{Conversion } (\%) = \frac{\text{moles of sorbitol consumed}}{\text{moles of sorbitol initially charged}} * 100 \quad (1)$$

$$C_{liq}\ (\%mol_C) = \frac{\text{moles of carbon in all detected products in liquid phase}}{\text{moles of carbon initially charged}} * 100 \quad (2)$$

$$C_{gas}\ (\%mol_C) = \frac{\text{moles of carbon in all detected products in gaseous phase}}{\text{moles of carbon initially charged}} * 100 \quad (3)$$

At the end of the test (i.e., after 6 h of reaction), after cooling of the autoclave, the catalysts were recovered by decantation and washed with water, and then dried overnight at 120 °C. The analyses of the carbon and hydrogen contents of the residues deposited on the used catalysts were performed on a NA 2100 PROTEIN equipment from Thermoquest (coupled with the Eager 2000 software, version 2000, ThermoFisher Scientific, Courtaboeuf, France), by total combustion of the sample (approximately 1–2 mg) under a He/O_2 mixture at 1020 °C. The CO_2 and H_2O formed were led on an active carbon column and quantified by a TCD detector, the weight contents being obtained with a relative uncertainty of 5%.

4. Conclusions

This study followed on from our previous work [25] devoted to sorbitol transformation to hexane on bifunctional Ru–Pt/S40 catalytic systems constituted of 3 wt.% Pt and 3 wt.% Ru and synthetized by three preparation methods, namely co-impregnation (CI), successive impregnations (SI) and catalytic reduction deposition (CR). The objective of the present study was then to attempt to prepare other bimetallic Ru–Pt catalysts by varying (i) the order of impregnation of the precursor salts by the SI method and (ii) the Ru content deposited by the CR method recognized to favor the interaction between the metals. New SI–(Pt–Ru)/S40 and CR–(x%Ru–Pt)/S40 (with x = 2, 1 or 0.5 wt.%Ru) bimetallic

catalysts were then prepared and evaluated for sorbitol transformation under similar experimental conditions to our previous experiment (10 wt.% sorbitol aqueous solution, 240 °C, 60 bar under H_2 atmosphere). All of the studied Ru–Pt/S40 catalysts were fully characterized in order to find a correlation between their morphology and their catalytic performances.

The existence of a Pt–Ru interaction was demonstrated on all the SI and CR samples, confirming that both these methods favor the formation of bimetallic particles, which is not the case with the CI method. However with the CR method, the Ru atoms tend to form isolated agglomerates on the support when the additive is introduced in high quantity (3 wt.%). Moreover, the total acidity of the bimetallic CR catalysts increases with the Ru content with a Brønsted acidity more marked for 0.5 and 1 wt.% Ru contents. XPS analysis revealed also that the chemical nature of the Ru species differs on the different bimetallic catalysts according to the synthesis method. Indeed, while Pt was in the Pt^0 metallic state on all reduced samples, metallic (Ru^0) and oxidized (Ru^{4+}) species were observed on the SI–(Ru–Pt)/S40 and CR catalysts. On the contrary, only Ru^0 species were identified on the CI catalyst, such as on the Ru/S40 monometallic catalyst. The presence of a PtRu alloy in the SI–(Ru–Pt)/S40 and CR catalysts was finally assumed from the XRD and XPS analyses.

Concerning the performances for sorbitol transformation, the SI–(Pt–Ru)/S40 sample was observed to be as poorly selective to hexane as the CI catalyst, which is certainly due to the presence of large particles on this system displaying a Pt–Ru interaction. The CR–(Ru–Pt)/S40 bimetallic catalysts showed different performances depending on the Ru content, with an optimum yield to hexane obtained for 1 wt.% Ru deposited by catalytic reduction deposition. Finally, among all the studied catalysts, the SI–(Ru–Pt)/S40 bimetallic system appeared as the most selective sample to convert sorbitol to hexane. The synergistic effect on the SI–(Ru–Pt)/S40 catalyst for producing C6 hydrocarbons was attributed to the presence of bimetallic particles of small size on this catalyst favoring an electronic exchange from Ru to Pt.

We concluded that the aqueous phase conversion of sorbitol to hexane involves two pathways, the former including the formation of isosorbide and the latter that of C6 furanic compounds (2,5-DMF and 2,5-DMTHF, more reactive than isosorbide and more selectively convertible to hexane). The Pt metal phase then promotes the "isosorbide" route and the Ru phase the "furanic" one. Thus, according to the equilibrium obtained between bimetallic function and acidic function (in particular relative to the Brønsted acidic sites), the Ru–Pt/S40 bimetallic catalysts follow a combination of both reaction pathways that influences the hexane yield. The system prepared by successive impregnations of Pt and then Ru appears as the bimetallic catalyst having the best metal–acid function balance leading to a hexane yield of 24.4 mol_C% for 80% sorbitol conversion. During the sorbitol transformation under hydrothermal conditions, this catalyst underwent sintering of these metal particles as well as a poisoning by coke deposition, but to a lesser extent with respect to the Pt/S40 reference system.

Supplementary Materials: The following are available online at http://www.mdpi.com/2073-4344/9/2/146/s1. Figure S1. NH3–TPD profiles of the monometallic Ru/S40 and Pd/S40 catalysts, and of the Ru-Pt/S40 bimetallic catalysts prepared by: (a) catalytic reduction deposition (CR); (b) co-impregnation (CI) and successive impregnations (SI), Table S1: Carbon distribution in the liquid and gas phases at 80-96% of sorbitol conversion for the Pt and Ru based catalysts supported on S40 prepared by successive impregnations (SI) and co-impregnation (CI). Conditions: 10 wt.% sorbitol solution, 240 °C, 60 bar under H2, Table S2: Carbon distribution in the liquid and gas phases at 80-96% of sorbitol conversion for the Pt and Ru based catalysts supported on S40 prepared by catalytic reduction deposition (CR). Conditions: 10 wt.% sorbitol solution, 240 °C, 60 bar under H_2.

Author Contributions: D.M. performed the experiments and analyzed the data; L.V. and C.E. supervised the research activity; C.E., L.V. and D.M. wrote the manuscript; C.C. contributed with XPS characterization and analysis of the obtained spectra.

Funding: This research received no external funding.

Acknowledgments: The authors thank the European community (FEDER) and the "Région Nouvelle Aquitaine" for their financial support.

Conflicts of Interest: The authors declare no conflict of interest.

References

1. Davda, R.R.; Shabaker, J.W.; Huber, G.W.; Cortright, R.D.; Dumesic, J.A. A review of catalytic issues and process conditions for renewable hydrogen and alkanes by aqueous-phase reforming of oxygenated hydrocarbons over supported metal catalysts. *Appl. Catal. B Environ.* **2005**, *56*, 171–186. [CrossRef]
2. Huber, G.W.; Iborra, S.; Corma, A. Synthesis of transportation fuels from biomass: Chemistry, catalysts, and engineering. *Chem. Rev.* **2006**, *106*, 4044–4098. [CrossRef] [PubMed]
3. Chheda, J.N.; Huber, G.W.; Dumesic, J.A. Liquid-phase catalytic processing of biomass-derived oxygenated hydrocarbons to fuels and chemicals. *Angew. Chem. Int. Ed. Engl.* **2007**, *46*, 7164–7183. [CrossRef] [PubMed]
4. Alonso, D.M.; Bond, J.Q.; Dumesic, J.A. Catalytic conversion of biomass to biofuels. *Green Chem.* **2010**, *12*, 1493–1513. [CrossRef]
5. Nakagawa, Y.; Liu, S.; Tamura, M.; Tomishige, K. Catalytic total hydrodeoxygenation of biomass-derived polyfunctionalized substrates to alkanes. *ChemSusChem* **2015**, *8*, 1114–1132. [CrossRef] [PubMed]
6. Guo, M.; Song, W.; Buhain, J. Bioenergy and biofuels: History, status, and perspective. *Renew. Sustain. Energy Rev.* **2015**, *42*, 712–725. [CrossRef]
7. Deneyer, A.; Ennaert, T.; Cavents, G.; Dijkmans, J.; Vanneste, J.; Courtin, C.M.; Dusselier, M.; Sels, B.F. Compositional and structural feedstock requirements of a liquid phase cellulose-to-naphtha process in a carbon- and hydrogen-neutral biorefinery context. *Green Chem.* **2016**, *18*, 5594–5606. [CrossRef]
8. Alonso, D.M.; Wettstein, S.G.; Dumesic, J.A. Bimetallic catalysts for upgrading of biomass to fuels and chemicals. *Chem. Soc. Rev.* **2012**, *41*, 8075–8098. [CrossRef]
9. Werpy, T.; Petersen, G.; Aden, A.; Bozell, J.; Holladay, J.; Manheim, A.; Eliot, D.; Lasure, L.; Jones, S. *Top Value Added Chemicals from Biomass*; U.S. Department of Energy: Oak Ridge, TN, USA, 2004; Volume 1.
10. Bozell, J.J.; Petersen, G.R. Technology development for the production of biobased products from biorefinery carbohydrates—the US Department of Energy's "Top 10" revisited. *Green Chem.* **2010**, *12*, 539–554. [CrossRef]
11. Zhang, J.; Li, J.; Wu, S.-B.; Liu, Y. Advances in the catalytic production and utilization of sorbitol. *Ind. Eng. Chem. Res.* **2013**, *52*, 11799–11815. [CrossRef]
12. Jia, Y.; Liu, H. Mechanistic insight into the selective hydrogenolysis of sorbitol to propylene glycol and ethylene glycol on supported Ru catalysts. *Catal. Sci. Technol.* **2016**, *6*, 7042–7052. [CrossRef]
13. Cortright, R.D.; Davda, R.R.; Dumesic, J.A. Hydrogen from catalytic reforming of biomass-derived hydrocarbons in liquid water. *Nature* **2002**, *418*, 964–967. [CrossRef] [PubMed]
14. Huber, G.W.; Cortright, R.D.; Dumesic, J.A. Renewable alkanes by aqueous-phase reforming of biomass-derived oxygenates. *Angew. Chem. Int. Ed.* **2004**, *43*, 1549–1551. [CrossRef] [PubMed]
15. Li, N.; Huber, G.W. Aqueous-phase hydrodeoxygenation of sorbitol with Pt/SiO_2–Al_2O_3: Identification of reaction intermediates. *J. Catal.* **2010**, *270*, 48–59. [CrossRef]
16. Moreno, B.M.; Li, N.; Lee, J.; Huber, G.W.; Klein, M.T. Modeling aqueous-phase hydrodeoxygenation of sorbitol over Pt/SiO_2–Al_2O_3. *RSC Adv.* **2013**, *3*, 23769–23784. [CrossRef]
17. West, R.M.; Tucker, M.H.; Braden, D.J.; Dumesic, J.A. Production of alkanes from biomass derived carbohydrates on bi-functional catalysts employing niobium-based supports. *Catal. Commun.* **2009**, *10*, 1743–1746. [CrossRef]
18. Li, N.; Tompsett, G.A.; Huber, G.W. Renewable high-octane gasoline by aqueous-phase hydrodeoxygenation of C_5 and C_6 carbohydrates over Pt/zirconium phosphate catalysts. *ChemSusChem* **2010**, *3*, 1154–1157. [CrossRef]
19. Kim, Y.T.; Dumesic, J.A.; Huber, G.W. Aqueous-phase hydrodeoxygenation of sorbitol: A comparative study of Pt/Zr phosphate and Pt-ReO_x/C. *J. Catal.* **2013**, *304*, 72–85. [CrossRef]
20. West, R.M.; Kunkes, E.L.; Simonetti, D.A.; Dumesic, J.A. Catalytic conversion of biomass-derived carbohydrates to fuels and chemicals by formation and upgrading of mono-functional hydrocarbon intermediates. *Catal. Today* **2009**, *147*, 115–125. [CrossRef]
21. Lee, J.; Kim, Y.T.; Huber, G.W. Aqueous-phase hydrogenation and hydrodeoxygenation of biomass-derived oxygenates with bimetallic catalysts. *Green Chem.* **2014**, *16*, 708–718. [CrossRef]
22. Neira D'Angelo, M.F.; Ordomsky, V.; van der Schaaf, J.; Schouten, J.C.; Nijhuis, T.A. Continuous hydrogen stripping during aqueous phase reforming of sorbitol in a washcoated microchannel reactor with a Pt–Ru bimetallic catalyst. *Int. J. Hydrog. Energy* **2014**, *39*, 18069–18076. [CrossRef]

23. Soares, A.V.H.; Perez, G.; Passos, F.B. Alumina supported bimetallic Pt–Fe catalysts applied to glycerol hydrogenolysis and aqueous phase reforming. *Appl. Catal. B Environ.* **2016**, *185*, 77–87. [CrossRef]
24. Jin, X.; Thapa, P.S.; Subramaniam, B.; Chaudhari, R.V. Kinetic modeling of sorbitol hydrogenolysis over bimetallic RuRe/C catalyst. *ACS Sustain. Chem. Eng.* **2016**, *4*, 6037–6047. [CrossRef]
25. Messou, D.; Vivier, L.; Especel, C. Sorbitol transformation over bimetallic Ru-Pt/SiO_2-Al_2O_3 catalysts: Effect of the preparation method. *Energy Convers. Manag.* **2016**, *127*, 55–65. [CrossRef]
26. Epron, F.; Especel, C.; Lafaye, G.; Marécot, P. *Nanoparticles and Catalysis*; Astruc, D., Ed.; Wiley-VCH verlag GmbH &, Co.: Weinheim, Germany, 2008; pp. 279–302.
27. Ly, B.K.; Tapin, B.; Aouine, M.; Delichere, P.; Epron, F.; Pinel, C.; Especel, C.; Besson, M. Insights into the oxidation state and location of rhenium in Re-Pd/TiO_2 catalysts for aqueous-phase selective hydrogenation of succinic acid to 1,4-butanediol as a function of palladium and rhenium deposition methods. *ChemCatChem* **2015**, *7*, 2161–2178. [CrossRef]
28. Jovanovič, P.; Selih, V.S.; Sala, M.; Hocevar, S.; Ruiz-Zepeda, F.; Hodnik, N.; Bele, M.; Gaberscek, M. Potentiodynamic dissolution study of PtRu/C electrocatalyst in the presence of methanol. *Electrochim. Acta* **2016**, *211*, 851–859. [CrossRef]
29. AlYami, N.M.; LaGrow, A.P.; Joya, K.S.; Hwang, J.; Katsiev, K.; Anjum, D.H.; Losovyj, Y.; Sinatra, L.; Kim, J.Y.; Bakr, O.M. Tailoring ruthenium exposure to enhance the performance of fcc platinum@ruthenium core–shell electrocatalysts in the oxygen evolution reaction. *Phys. Chem. Chem. Phys.* **2016**, *18*, 16169–16178. [CrossRef] [PubMed]
30. Mazzieri, V.; Coloma-Pascual, F.; Arcoya, A.; L'Argentière, P.C.; Figoli, N.S. XPS, FTIR and TPR characterization of Ru/Al_2O_3 catalysts. *Appl. Surf. Sci.* **2003**, *210*, 222–230. [CrossRef]
31. Wang, H.; Chen, S.; Wang, C.; Zhang, K.; Liu, D.; Haleem, Y.A.; Zheng, X.; Ge, B.; Song, L. Role of Ru oxidation degree for catalytic activity in bimetallic Pt/Ru nanoparticles. *J. Phys. Chem. C* **2016**, *120*, 6569–6576. [CrossRef]
32. Velazquez-Palenzuela, A.; Centellas, F.; Garrido, J.A.; Arias, C.; Rodriguez, R.M.; Brillas, E.; Cabot, P.-L. Structural properties of unsupported Pt−Ru nanoparticles as anodic catalyst for proton exchange membrane fuel cells. *J. Phys. Chem. C* **2010**, *114*, 4399–4407. [CrossRef]
33. Lafaye, G.; Ekou, T.; Micheaud-Especel, C.; Montassier, C.; Marécot, P. Citral hydrogenation over alumina supported Rh-Ge catalysts: Effects of the reduction temperature. *Appl. Catal. A Gen.* **2004**, *257*, 107–117. [CrossRef]
34. Kemball, C.; Leach, H.F.; Skundric, B.; Taylor, K.C. Reactions of 3,3-dimethylbut-1-ene with deuterium oxide or deuterium over oxide catalysts. *J. Catal.* **1972**, *27*, 416–423. [CrossRef]
35. John, C.S.; Kemball, C.; Rajadhayarsha, R.A. The mechanisms of dimethylbutene isomerization over alumina. *J. Catal.* **1979**, *57*, 264–271. [CrossRef]
36. Pines, H.J. Use of organic probes in detecting active sites in heterogeneous catalysis. *J. Catal.* **1982**, *78*, 1–16. [CrossRef]
37. Martin, D.; Duprez, D. Evaluation of the acid-base surface properties of several oxides and supported metal catalysts by means of model reactions. *J. Mol. Catal. A Chem.* **1997**, *118*, 113–128. [CrossRef]
38. Chia, M.; Pagán-Torres, Y.J.; Hibbitts, D.; Tan, Q.; Pham, H.N.; Datye, A.K.; Neurock, M.; Davis, R.J.; Dumesic, J.A. Selective Hydrogenolysis of polyols and cyclic ethers over bifunctional surface sites on rhodium–rhenium catalysts. *J. Am. Chem. Soc.* **2011**, *133*, 12675–12689. [CrossRef] [PubMed]
39. Zhang, L.; Karim, A.M.; Engelhard, M.H.; Wei, Z.; King, D.L.; Wang, Y. Correlation of Pt–Re surface properties with reaction pathways for the aqueous-phase reforming of glycerol. *J. Catal.* **2012**, *287*, 37–43. [CrossRef]
40. Maris, E.P.; Ketchie, W.C.; Murayama, M.; Davis, R.J. Glycerol hydrogenolysis on carbon-supported PtRu and AuRu bimetallic catalysts. *J. Catal.* **2007**, *251*, 281–294. [CrossRef]
41. Kirilin, A.V.; Tokarev, A.V.; Murzina, E.V.; Kustov, L.M.; Mikkola, J.-P.; Murzin, D.Y. Reaction products and transformations of intermediates in the aqueous-phase reforming of sorbitol. *ChemSusChem* **2010**, *3*, 708–718. [CrossRef]
42. Zhao, L.; Zhou, J.H.; Sui, Z.J.; Zhou, X.G. Hydrogenolysis of sorbitol to glycols over carbon nanofiber supported ruthenium catalyst. *Chem. Eng. Sci.* **2010**, *65*, 30–35. [CrossRef]
43. Banu, M.; Sivasanker, S.; Sankaranarayanan, T.M.; Venuvanalingam, P. Hydrogenolysis of sorbitol over Ni and Pt loaded on NaY. *Catal. Commun.* **2011**, *12*, 673–677. [CrossRef]

44. Vilcocq, L.; Cabiac, A.; Especel, C.; Lacombe, S.; Duprez, D. New insights into the mechanism of sorbitol transformation over an original bifunctional catalytic system. *J. Catal.* **2014**, *320*, 16–25. [CrossRef]
45. Sinfelt, J.H.; Yates, D.J.C. Catalytic hydrogenolysis of ethane over the noble metals of Group VIII. *J. Catal.* **1967**, *8*, 82–90. [CrossRef]
46. Tronci, S.; Pittau, B. Conversion of glucose and sorbitol in the presence of Ru/C and Pt/C catalysts. *RSC Adv.* **2015**, *5*, 23086–23093. [CrossRef]
47. Antolini, E.; Giorgi, L.; Cardellini, F.; Passalacqua, E. Physical and morphological characteristics and electrochemical behaviour in PEM fuel cells of PtRu /C catalysts. *J. Solid State Electrochem.* **2001**, *5*, 131–140. [CrossRef]
48. Douidah, A.; Marécot, P.; Labruquère, S.; Barbier, J. Stability of supported platinum catalysts in aqueous phase under hydrogen atmosphere. *Appl. Catal. A Gen.* **2001**, *210*, 111–120. [CrossRef]
49. Vilcocq, L.; Cabiac, A.; Especel, C.; Lacombe, S.; Duprez, D. Study of the stability of Pt/SiO_2–Al_2O_3 catalysts in aqueous medium: Application for sorbitol transformation. *Catal. Commun.* **2011**, *15*, 18–22. [CrossRef]
50. Pieck, C.L.; Marécot, P.; Barbier, J. Effect of Pt-Re interaction on sulfur adsorption and coke deposition. *Appl. Catal. A Gen.* **1996**, *145*, 323–334. [CrossRef]
51. Xi, J.; Xia, Q.; Shao, Y.; Ding, D.; Yang, P.; Liu, X.; Lu, G.; Wang, Y. Production of hexane from sorbitol in aqueous medium over $Pt/NbOPO_4$ catalyst. *Appl. Catal. B Environ.* **2016**, *181*, 699–706. [CrossRef]
52. Op de Beeck, B.; Dusselier, M.; Geboers, J.; Holsbeek, J.; Morré, E.; Oswald, S.; Giebeler, L.; Sels, B.F. Direct catalytic conversion of cellulose to liquid straight-chain alkanes. *Energy Environ. Sci.* **2015**, *8*, 230–240. [CrossRef]
53. Kunkes, E.L.; Simonetti, D.A.; Dumesic, J.A.; Pyrz, W.D.; Murillo, L.E.; Chen, J.G.; Buttrey, D.J. The role of rhenium in the conversion of glycerol to synthesis gas over carbon supported platinum–rhenium catalysts. *J. Catal.* **2008**, *260*, 164–177. [CrossRef]
54. Liu, S.; Okuyama, Y.; Tamura, M.; Nakagawa, Y.; Imai, A.; Tomoshige, K. Catalytic conversion of sorbitol to gasoline-ranged products without external hydrogen over Pt-modified Ir-ReO_x/SiO_2. *Catal. Today* **2016**, *269*, 122–131. [CrossRef]
55. Messou, D.; Vivier, L.; Especel, C. Sorbitol transformation into biofuels over bimetallic platinum based catalysts supported on SiO_2-Al_2O_3—Effect of the nature of the second metal. *Fuel Proc. Technol.* **2018**, *177*, 159–169. [CrossRef]